Available online at www.sciencedirect.com
ScienceDirect
Journal of the European Ceramic Society 31 (2011) 2013–2022
www.elsevier.com/locate/jeurceramsoc

Effects of ZnO on the dielectric, conductive and piezoelectric properties of low-temperature-sintered PMnN-PZT based hard piezoelectric ceramics

Cheng-Che Tsai [a], Sheng-Yuan Chu [b,*], Cheng-Shong Hong [c], Shih-Fang Chen [d]

[a] Department of Electronics and Computer science, Tung-Fang Design University, Kaohsiung 829, Taiwan
[b] Department of Electrical Engineering, National Cheng Kung University, Tainan 701, Taiwan
[c] Department of Electronic Engineering, National Kaohsiung Normal University, Kaohsiung 824, Taiwan
[d] Department of Electronic Engineering, Southern Taiwan University, Tainan County 710, Taiwan

Received 29 July 2010; received in revised form 22 March 2011; accepted 3 April 2011
Available online 18 May 2011

Abstract

The ZnO-doped $Pb_{0.98}Ca_{0.01}Sr_{0.01}[(Mn_{1/3}Nb_{2/3})_{0.06}–(Zr_{0.52}Ti_{0.48})_{0.94}]O_3 + 0.15$ wt.% CuO for varying amounts of ZnO (x wt.%) ceramics were prepared. Their structure evolutions and electrical properties were systematically investigated. A dc and ac conductivity analysis was conducted. It demonstrated that the probability of ZnO dopants entered the A and/or B-site of the perovskite structure, which affected the dielectric relaxation, activation energy, and piezoelectric properties. Experimental results showed that the tetragonality of the perovskite structure and electro-mechanical energy transformation ratio (k^2 value) were increased with increasing the ZnO contents for $0.1 \leqq x \leqq 0.5$. As ZnO contents increased for $0.1 \leqq x \leqq 2$, the diffused phase transition (DPT) characteristic was gradually disappeared. And, the ac activation energy calculated was also decreased due to the conduction mechanism. In addition, the frequency dependence of the ac conductivity was complied with the Jonscher power law, for $x = 0.5$, 1, and 1.5 at measured temperature.

Keywords: Piezoelectric activity; Activation energy; Diffusive exponent; Perovskite structure

1. Introduction

Piezoelectric lead zirconate titanate (PZT) have been extensively used in piezoelectric devices because of its good electro-mechanical properties near the morphotropic phase boundary (MPB) region.[1,2] However, to meet the higher performance requirements of piezoelectric devices, many aliovalent additions to PZT network system enhance the "soft" or/and "hard" effect to improve the piezoelectric activity. High values for the electro-mechanical coupling factor (k) and the high mechanical quality factor (Q) ensure the maximum electro-mechanical transformation.[1] For the piezoelectric material systems, the modified PMnN-PZT piezoelectric material meets the above-mentioned requirements and its piezoelectric properties are superior to those for Mn-, Nb-doped PZT.[3,4] PMnN-PZT based piezoelectric material systems are extensively used in motors, transformers, therapeutic transducers, sensors and actuators because they are adaptable enough to allow fabrication of devices with higher performance characteristics.[5–8]

Lead-free NKN and BNT based systems provide an environmentally friendly alternative to the PZT-based materials. However, they are difficult to fabricate, with high k (e.g. $k_p > 0.50$) and Q (e.g. $Q_m > 1000$) as hard piezoelectric ceramics for applications in high power transducers. Therefore, the development of low-temperature-sintered PZT based piezoelectric materials is becoming important. It is reported in literature that CuO, as an additive, lowers the sintering temperature and increases the sintering density of piezoelectric ceramics.[9–13] Further lowering of the sintering temperature requires the addition of greater amounts of CuO, but this causes a corresponding degradation in the piezoelectric properties. Co-doping using CuO and another metal oxide or dioxide, such as ZnO, Li_2CO_3, MnO_2, etc. to lower the sintering temperature below 1000 °C is used for the fabrication of low-temperature-sintered piezoelectric ceramics.

In this paper, the ZnO dopant is chosen as the co-doping element, based on the findings in literatures. Ha et al. reported

* Corresponding author. Tel.: +886 6 2757575x62381; fax: +886 6 2345482.
E-mail address: chusy@mail.ncku.edu.tw (S.-Y. Chu).

0955-2219/$ – see front matter © 2011 Elsevier Ltd. All rights reserved.
doi:10.1016/j.jeurceramsoc.2011.04.022

that the dielectric constant, electro-mechanical coupling factor and piezoelectric charge coefficient could be improved by doping suitable ZnO.[14] Ahn et al. showed that ZnO was effective in reducing the sintering temperature to 950 °C, with the retention of good piezoelectric properties.[15] Yoon et al. showed that ZnO could increase the piezoelectric voltage output coefficient and piezoelectric charge constant.[16] Rubio-Marcos et al. investigated the effect of ZnO on structural evolutions and electrical properties for the lead-free (K,Na,Li)(Nb,Ta,Sb)O_3 system.[17] However, these studies seldom refer to the probability of ZnO dopants entered the A and/or B-site of the perovskite structure, affecting the dielectric relaxation, activation energy, and piezoelectric properties of low-temperature sintered piezoelectric ceramics.

Using the results of previous research on the properties of low-temperature-sintered CuO-doped $Pb_{0.98}Ca_{0.01}Sr_{0.01}[(Mn_{1/3}Nb_{2/3})_{0.06}–(Zr_{0.52}Ti_{0.48})_{0.94}]O_3$ (PMNZT-C) ceramics, they exhibited good dielectric and piezoelectric properties for making the SAW device substrate,[7] but improvements to electro-mechanical properties are possible and the physical properties are worthy of further study. Recently, a combination method, using mixed oxides and wolframite (abbreviated as modified mixed-oxide method), has been used in PZN–PZT based material systems to improve the dielectric and piezoelectric properties, and the elimination of the second phase as reported in literatures.[18,19]

This study investigated the characteristics of ZnO additives into a PMNZT-C piezoelectric ceramics material system, using the modified mixed-oxide method, in order to exploit the physical properties of low sintering temperature (<1000 °C) ceramics and to demonstrate, using conductivity analysis, that ZnO dopants entering the sites of a crystal structure (i.e. A or/and B site) affect the electrical properties of the material. In addition, the effect of doping on the dielectric relaxation and conductivity behavior by progressively introducing doping amounts of ZnO into the PMNZT-C ceramics.

2. Experimental

The compositions chosen for the present study were $Pb_{0.98}Ca_{0.01}Sr_{0.01}[(Mn_{1/3}Nb_{2/3})_{0.06}–(Zr_{0.52}Ti_{0.48})_{0.94}]O_3$ + 0.15 wt.% CuO (PMNZT-C) + x wt.% ZnO ($0 \leqq x \leqq 2$) (abbreviated as PMNZT-CZ10x). Specimens were prepared with different compositions to improve the sintering density and to achieve the optimum piezoelectric properties.

Commercially available oxide powders of PbO, $CaCO_3$, $SrCO_3$, Nb_2O_5, $MnCO_3$, ZrO_2, TiO_2, CuO and ZnO with purity > 99% were used as the starting materials. The perovskite structure was prepared using the modified mixed oxides method. The Wolframite precursor $(Zr_{0.52}Ti_{0.48})O_2$ was firstly calcined at 1400 °C for 4 h. Then, Nb_2O_5, $MnCO_3$, $CaCO_3$, $SrCO_3$, PbO, and $(Zr_{0.52}Ti_{0.48})O_2$ were then weighted by the mole ratio according to the given composition and ball-milled for 24 h. After drying, the powders were calcined at 880 °C for 3 h. Thereafter, CuO and ZnO were added to the calcined powders, and then were ball-milled for 24 h and were dried. After that, the 8 wt.% of PB72 and 40% distilled water, constituting a binder solution was added to the dried powders, and the mixture was granulated.

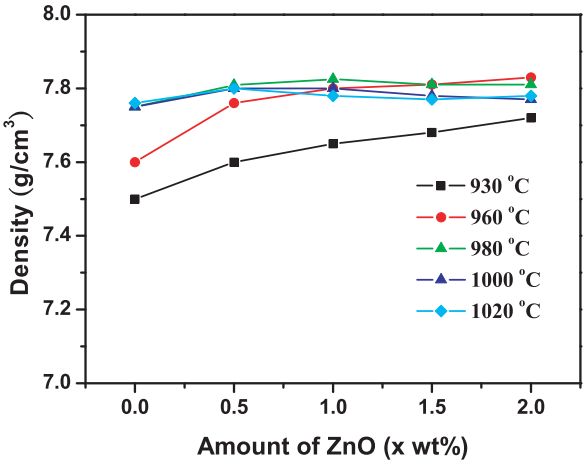

Fig. 1. The bulk density of PMNZT-CZ10x specimens versus the different sintering temperature.

The samples were pressed into disc shape 16 mm in diameter and 2.2 mm in thickness. Their forming average green density was 5.6 g/cm^3. The samples were sintered at 930–1020 °C for 4 h in a covered alumina crucible. The sintered pellets were polished into the desired thickness and were screen-printed with silver paste on both opposite faces, followed by firing 820 °C for 10 min. Then, the electroded samples were placed in silicon oil bath at 150 °C and poled in a DC electric field of 3 kV/mm, for 30 min.

The bulk densities of the polished pellets were measured by the Archimedes method. The compositional analyses of the sintered pellets were determined by X-ray diffraction (XRD) using a Seimens D-5000 diffractometer. The microstructure was analyzed by field emission scanning electron microscopy (FESEM) using a Hitachi S-4100 microscope. The Curie temperature (T_C) and the dielectric properties of un-poled specimens were measured using a HP-4192A impedance analyzer at 1 kHz, 10 kHz, 100 kHz, and a 0.5 V_{rms} oscillation signal in controlled furnace with heating rate of 1 °C/min from 20 °C to 450 °C. Simultaneously the temperature-dependent values of dc and ac conductivity were calculated.[20] The dc insulation resistance of un-poled specimens was measured at room temperature using an ohm meter (HIOKI SM-8215 super megaohm meter, HIOKI, Nagano, Japan) at room temperature.

To measure the piezoelectric properties, the poled specimens were aged for one week to obtain stable values. The resonance frequency, anti-resonance frequency and resonance resistance were then measured using an agilent 4294A precision impedance analyzer. The mechanical quality factor and electro-mechanical coupling factor were calculated using resonance and anti-resonance method, according to IEEE standards.[21]

3. Results and discussion

3.1. Phase evolution and microstructures

Fig. 1 shows the bulk densities of ZnO-added PMNZT-C specimens versus the sintering temperature. The bulk densities

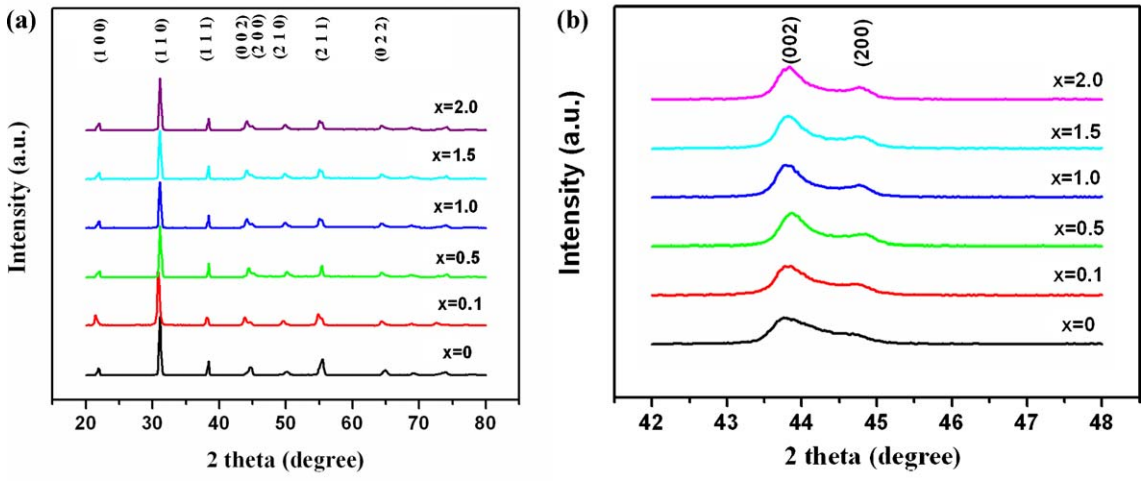

Fig. 2. X-ray diffraction patterns of specimens for PMNZT-CZ10x composition (a) in the 2θ range of 20–80° (b) enlarged (0 0 2) and (2 0 0) peaks within 42–48°.

of ZnO-doped PMNZT-C specimens increase with increasing the sintering temperature, reaching saturation between 980 °C and 1020 °C. For a given sintering temperature, the bulk density of ZnO-doped PMNZT-C specimen increases with increasing the amount of ZnO. It achieves a maximum value at $x = 1.5$, and then decreases. These results indicate that the addition of ZnO dopants can lower the sintering temperature and slightly increase the bulk density because the addition of ZnO probably facilitate the grain growth, resulting in much dense PMNZT-CZ10x specimens for $0 < x < 1.5$. However, further increasing the ZnO dopants will probably segregate at the grain boundary and inhibit the grain boundary diffusion, resulting in a gradual decrease in the bulk densities of specimens for $x > 1.5$. As the sintering temperature is between 980 °C and 1020 °C, the bulk densities of ZnO-doped specimens exhibit the maximum values between 7.82 and 7.85 g/cm^3, which is higher than values for un-doped PMNZT-C specimens. The effective sintering temperatures are between the range 980 °C–1020 °C. Thus, a sintering temperature of 980 °C is the preferred temperature for low temperature sintering (<1000 °C) for PMNZT-CZ10x compositions. It is probable that the oxygen vacancies producing are advantageous to processing of mass transport diffusion during sintering process or form the low temperature sintering aids to promote the densification of the specimens as reported in the literature.[22]

Fig. 2 shows the XRD patterns of the ZnO-doped PMNZT-C specimens and enlarged (2 0 0) peak patterns, for sintering at 980 °C. In these patterns, there is no obvious second phase ($Pb_3Nb_4O_{13}$), but the crystal structures of the specimens are slightly modified by the addition of ZnO as shown by the change of (0 0 2) and (2 0 0) peaks.

The perovskite phase appears to coexist with tetragonal phase and rhombohedral phase between 43 °C and 48 °C. These reflections of (0 0 2) and (2 0 0) peaks can be fitted to three Gaussian functions. The tetragonal phase fraction (F_T%) is calculated by the equation[23]

$$F_T\% = \frac{\{I_T(002) + I_T(200)\}}{\{I_T(002) + I_T(200) + I_R(200)\}} \times 100\%$$

where $I_T(0\,0\,2)$ and $I_T(2\,0\,0)$ are the intensities of tetragonal (0 0 2) and (2 0 0) reflections, and $I_R(2\,0\,0)$ is the intensity of the rhombohedral (2 0 0) reflection, respectively. The c/a ratio of crystal structures for PMNZT-CZ10x specimens are listed in Table 1. It is seen that the Zn ions exit mainly in Zn^{2+} state, which most likely enters into perovskite structure of BO_6 octahedron to substitute for the B-site ion of the perovskite structure, creating the oxygen vacancies and/or may substitute for the A-site of the perovskite structure to occupy the vacancies left by lead during the sintering process, resulting in structural deformation. This leads to the c/a ratio increase, and a slight shift in (0 0 2) and (2 0 0) reflection peaks toward the higher diffraction angle. Excess ZnO additive ($x > 1$) may segregate in the grain boundary resulting in a slight decrease in the c/a ratio as shown in Table 1. And, the reflection peaks (0 0 2) and (2 0 0) shift toward the lower diffraction angle as compared to the diffraction pattern for $x = 0.5$ in Fig. 2(b). The shifts in reflection peaks (0 0 2) and (2 0 0) directly influence the change in crystal structure. Therefore, using Goldschmidt's tolerance factor (t)[24,25] it is possible to estimate the amount of ZnO entering the A-site and/or B-site proportion of the crystal structure. Further investigation of this inference provides a basis for future study.

The SEM images of the fracture samples of ZnO-doped PMNZT-C are shown in Fig. 3. They demonstrate that the microstructures of ZnO doped PMNZT-C specimens become denser as the amount of ZnO increases, and the grain size increases with increasing the ZnO amount from 1.3–1.8 μm for $x = 0$, to 2.2–3.2 μm for $x = 2$. The distributions of grain size for PMNZT-CZ10x specimens are shown in Fig. 4. From Figs. 3 and 4, they show that the suitable ZnO additives ($x \leqq 0.5$) will facilitate the grain growth, but excess amounts of ZnO additive ($x > 0.5$) will probably segregate at the grain boundary and inhibit local grain growth leading to a broader distribution of grain size.

The grain boundary evolution presents intergranula for $x = 0$–0.5, intergranula and intragranula for $x = 0.5$–1.5, and intragranula for $x = 2$. In other words, a homogeneous structure can be observed for $x \leqq 0.5$, and inhomogeneous structures are gradually formed as $x > 0.5$ due to the more ZnO amounts pos-

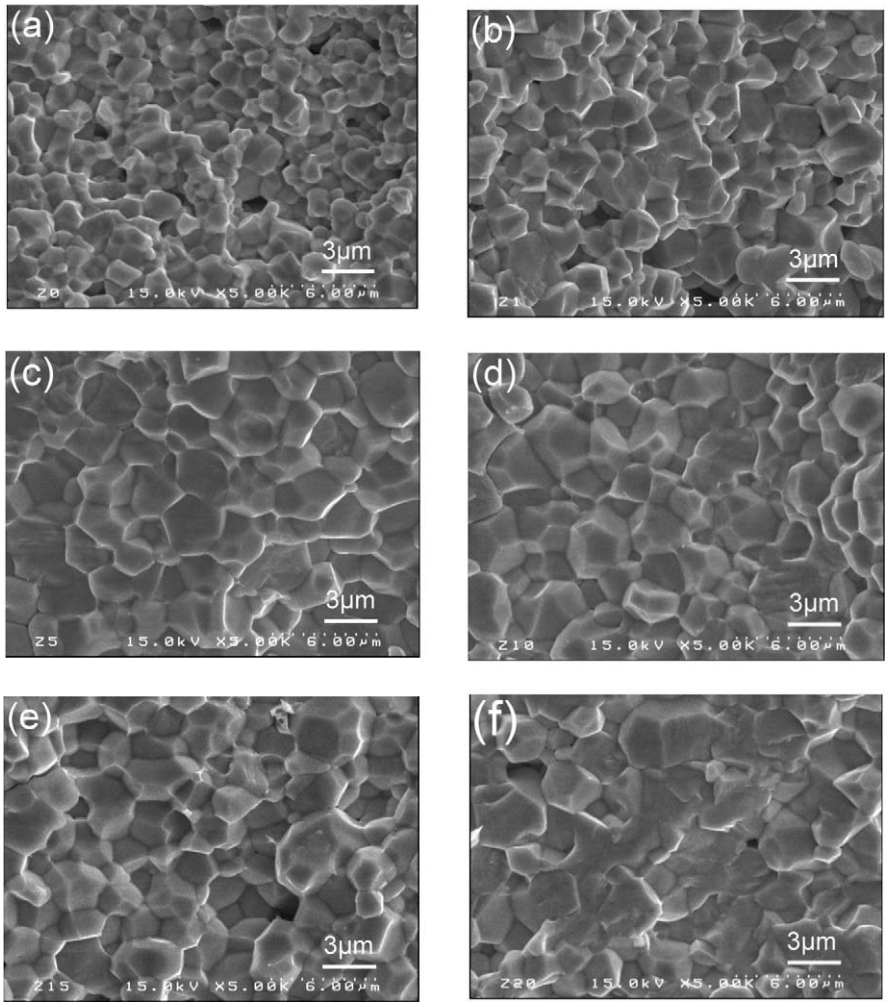

Fig. 3. The SEM image of the fracture samples of PMNZT-CZ10x composition with ZnO contents (x wt.%) (a) $x=0$ (b) $x=0.1$ (c) $x=0.5$ (d) $x=1$ (e) $x=1.5$ (f) $x=2$.

sibly segregating at the grain boundary to form a liquid phase of a mixture of CuO and ZnO or CuO, ZnO, MnO and Nb_2O_5 resulting in the abnormal grain growth. This phenomenon is consistent with the results reported by Park et al. and Li et al. in literatures.[26,27]

3.2. Dielectric properties

The dielectric constant and dielectric loss for PMNZT-CZ10x specimens as a function of the amount of ZnO additive, using the modified mixed oxide method, measured at a frequency of 1 kHz and at room temperature are listed in Table 2. It can be seen that the dielectric constant increases with increasing ZnO content and achieves the maximum value at $x=0.5$, and then decrease. Meanwhile, the dielectric loss increases with increasing ZnO content.

The trend of dielectric constant as a function of ZnO dopants is consistent with that of grain growth. It can be attributed to the two factors: (1) the increase of grain size as the amount of ZnO additive increases, causing increased polarization and easy domain wall motion shift, resulting in increases in both dielectric constant and dielectric loss and (2) increased dc conductivity leading to increases in both the dielectric constant and dielectric loss due to the intrinsic effect (volume effect).[28,29] As the amount of ZnO exceeds the solubility limit, it will segregate at grain boundary, hindering the domain wall switching, which results in a decrease in the dielectric constant due to the extrinsic contribution in the dielectric constant decrease.[29,30]

Table 1
The fraction of tetragonal phase (F_T%) calculated and the c/a ratio of crystal structure of PMNZT-CZ10x specimens.

Parameters	ZnO (x) additive				
x (wt.%)	0	0.1	0.5	1	2
Fraction of the tetragonal phase (F_T%)	70.6	75.3	79.6	79.5	78.8
c/a ratio of the crystal structure	1.019	1.020	1.0213	1.0212	1.0206

Table 2
Comparisons of ε_{max}, T_C and γ for the amount of ZnO in the PMNZT-CZ10x specimens.

Parameters	ZnO (x) additive				
x (wt.%)	0	0.1	0.5	1	2
ε_{max}	8058.6	12261.5	19516.3	18255.6	17131.7
T_C (°C)	342	348	329	320	338
γ	1.95	1.56	1.30	1.28	1.06

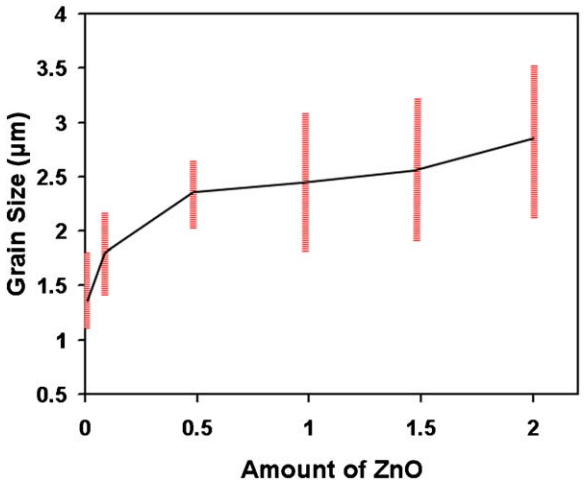

Fig. 4. The grain size distribution of specimens for PMNZT-CZ10x composition as a function of ZnO amounts.

Fig. 5 shows the temperature dependence of the dielectric constant, measured at a frequency of 10 kHz for PMNZT-CZ10x specimens sintered at 980 °C. For the PMNZT-CZ10x specimens, the dielectric constant peak increase with increasing the amount of ZnO additive, reaching a maximum value at $x = 0.5$. The dielectric peak at the Curie point also increases. These results demonstrate that the improved densification and increased grain size, caused by the ZnO doping, contribute to the dielectric peak.[13,29] In addition, the change in the Curie temperature for the specimens evidences the deformation of crystal structure (i.e. c/a ratio variation) and material composition dependence, which affects the Curie point and dielectric

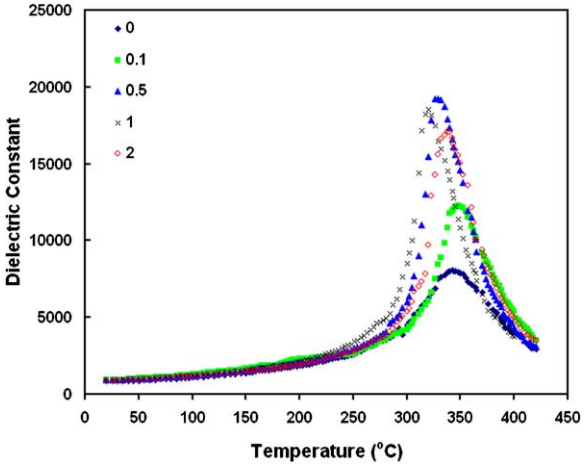

Fig. 5. Temperature dependence of dielectric constant versus the amount of ZnO additive for PMNZT-CZ10x specimens at measured frequency of 1 kHz.

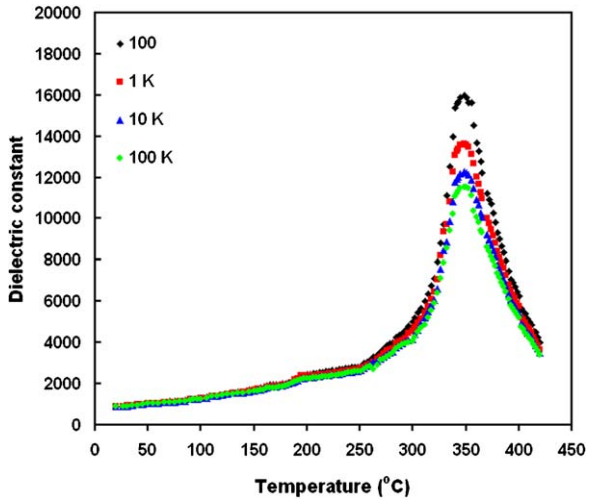

Fig. 6. Temperature dependence of dielectric constant at different measurement frequency for PMNZT-CZ10x specimens at $x = 0.1$.

constant. These physical properties listed in Tables 2–4 are similar to our reported paper[12] and other related literatures.[15,16]

To investigate the frequency dispersion, the dielectric constant as a function of the temperature, at different frequency, for $x = 0.1$ specimens shown in Fig. 6. The maximum dielectric constant peaks do not show an obvious shift at frequencies 100 Hz, 1 kHz, 10 kHz, and 100 kHz. The same phenomenon is also observed for other PMNZT-CZ10x specimens.

However, with the exception of $x = 2$, the dielectric peak in composition PMNZT-CZ10x is found to be broader, indicating the existence of diffuse phase transition (DPT). Increasing the amount of ZnO additive, the characteristics of the phase transition changes from the diffuse phase ($x = 0$) with a typical of short range order (SRO) to a normal ferroelectrics ($x = 2$) with long range order (LRO) characteristic, as seen in Fig. 5.

The degree of disorder or diffusiveness exponent (γ) for PMNZTC-Z10x specimens is estimated using an empirical formula proposed by Uchino and Nomura as follows[31]:

$$\frac{1}{\varepsilon} - \frac{1}{\varepsilon_m} = \frac{(T - T_m)^\gamma}{C}$$

where γ and C are assumed to be constants independent of temperature, and the value of γ is common between 1 and 2. The limit of $\gamma = 1$ make the equation fit the conventional Curie–Weiss law for normal ferroelectrics, and $\gamma = 2$ makes the equation fit the quadratic valid for the complete diffuse phase transition. While the γ value between 1 and 2 corresponds a so-called incomplete diffuse phase transition where the correlated ferroelectric clusters are hypothesized.

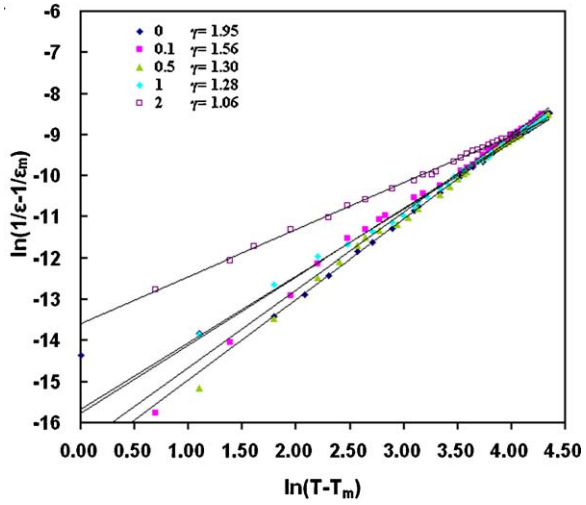

Fig. 7. The $\ln(1/\varepsilon - 1/\varepsilon_m)$ as a function of $\ln(T - T_m)$ at different amounts of ZnO additive for PMNZT-CZ10x specimens.

Fig. 7 shows the $\ln(1/\varepsilon - 1/\varepsilon_m)$ as a function of $\ln(T - T_m)$ at different ZnO additives of specimens for PMNZT-CZ10x composition. It can be observed that the diffusiveness exponent (γ) decreases with increasing the ZnO amount, which presents the PMNZTC-Z100x specimens from the broader distribution around the dielectric peak ($\gamma = 1.95$) at $x = 0$ to the normal ferroelectrics ($\gamma = 1.05$) at $x = 2$. It can be deduced that increased ZnO additive cause a decrease in the diffusiveness exponent (γ), inducing more ferroelectric clusters. This is evidenced by the enlarged (0 0 2) and (2 0 0) peaks in XRD patterns, which reveal the ZnO dopants have a tendency to stabilize the tetragonal structure. In addition, the maximum dielectric constant peak of the PMNZT-CZ10x specimens doesn't shift toward a higher temperature with increasing frequency. This result characterizes the phase transition as a DPT.

3.3. Electrical conductivity properties

The σ_{dc} (dc conductivity) and σ_{ac} (ac conductivity) of the PMNZT6-CZ10x specimens with respect to temperature and measured frequency can be calculated using the following relation[20]:

$$\sigma_{ac}(T, \omega) = \frac{t}{A}\omega\, C_p(\omega, T) \tan\delta(\omega, T)$$

$$\sigma_{dc} = \frac{t}{(R_b A)}$$

where t is the thickness of the specimen, A is the electrode area, ω is the measured angular frequency, C_p is the capacitance and $\tan\delta$ is the dielectric loss. R_b is the measured bulk resistance of specimen.

Fig. 8 shows the dc conductivity with the amount of ZnO additive for PMNZT-CZ10x specimens at room temperature. It can be seen that the dc conductivity at first decreases in region I (below 0.1 wt.%) because most of ZnO contents possibly enter the A-site of perovskite structure to occupy Pb vacancies, which results in the decreased conductivity of p-type ceramics. In this

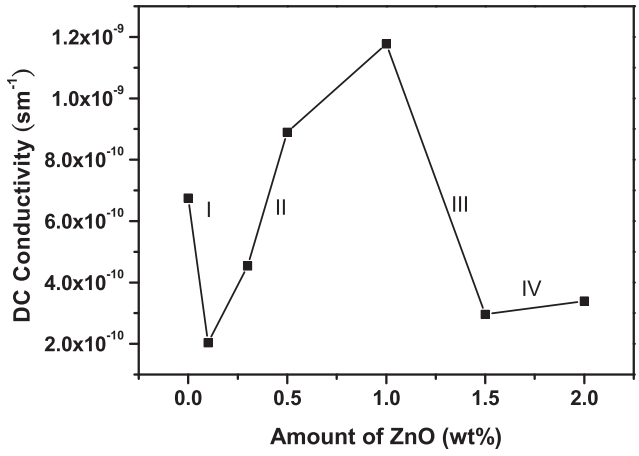

Fig. 8. dc conductivity as a function of ZnO amounts for PMNZT-CZ10x specimens at room temperature.

process, the number of lead vacancies is decreased, leading to a decrease in number of holes and a corresponding decrease, which transform neutral type ceramics. As the amount of ZnO is increased to 1 wt.% in region II, the conductivity is increased because most of the ZnO enters the B-site to produce the oxygen vacancies. This causes increased release of electrons to compensate for the valence deficiency of the B-site ions that are substituted by the ZnO additive, which increases the conductivity of the n-type. This reaction can be depicted using the Krogner–Vink symbolism as follows:

$$O_O \rightarrow \frac{1}{2}O_2(g) + V_O^x; \quad V_O^x \rightarrow V_O^{\bullet} + e^-; \quad V_O^{\bullet} \rightarrow V_O^{\bullet\bullet} + e^-$$

For amounts of ZnO additive below 1 wt.%, it can be speculated that ceramics that are originally p-type ceramics will transform into neutral type and then to n-type ceramics. As the amount of ZnO rises to between 1 wt.% and 1.5 wt.% in region III, it is possible that the excess Zn ions aggregate in the grain boundaries and change from the high valence to low valence. The reaction form can be depicted as:

$$Zn^{2+} + e^- \rightarrow Zn^+$$

which shows electron capture center and O^{-2} is attracted between the grain boundaries. This means that the grain boundary exhibits strong p-type conductivity, which counteracts the n-type conductivity, leading to a conductivity decrease. Further increasing the amounts of ZnO to more than 1.5 wt.% in region IV, more Zn ions aggregate in the grain boundary and play the role of p-type conductivity, resulting in an increase in conductivity. A similar phenomenon has been reported in the literatures.[32,33]

The change in the slope of conductivity versus temperature plot will reflect a change in the activation energy. Thus, their activation energy can be calculated from the slope of the conductivity versus temperature by Arrhenius law[34]:

$$\sigma = \sigma_0 \exp(-E_a/k_B T)$$

where σ is the conductivity, σ_0 is the pre-exponential factor, E_a is the activation energy, k_B is the Boltzmann constant

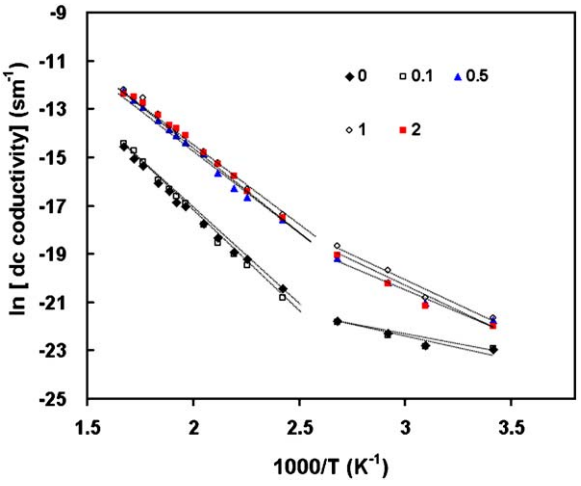

Fig. 9. dc conductivity as a function of 1000/T variation ranging from 300 °K to 600 °K for PMNZT-CZ10x specimens (symbols and dash line representing the experimental data and least square fit curve, respectively).

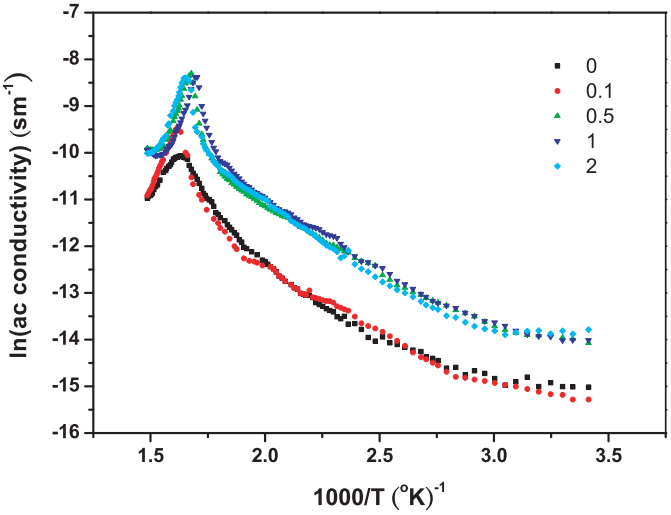

Fig. 10. ac conductivity versus the ZnO amounts as a function of 1000/T variation ranging from 300 °K to 600 °K for PMNZT-CZ10x specimens at measurement frequency of 10 kHz.

(8.617×10^{-5} eV K^{-1}), and T is the absolute temperature. For PMNZT-CZ10x, the temperature ($10^3/T$) dependence of σ_{dc} in the temperature range 30–280 °C is shown in Fig. 9.

The dc conductivity increases with increasing the temperature. Its value at the lower temperature depends on a hopping charge model, while at the medium temperature it depends on the polaron and oxygen vacancy conduction model. The slope of the curve represents the different dc activation energies and can be broadly divided into two regions 30–100 °C (lower temperature range) and 120–300 °C medium temperature range). The value of the dc activation energy (E_a), listed in Table 3, is calculated by the Matlab software using the least square approximation compared with Arrhenius law. It can be seen that the dc activation energy increases with the amount of ZnO additive in temperature range 30–100 °C, except for $x = 0.1$, while in the temperature range 120–300 °C, the dc activation energy increases with the increase in the amount of ZnO, and achieves the maximum value at $x = 0.1$, then decreases as $x > 0.1$. It can be seen that the dc activation energy with temperature for PMNZT-CZ10x specimens exhibits different trends in two separate temperature range 30–100 °C and 120–280 °C. It is speculated the variation in activation energy with temperature depends on the conduction mechanism and material composition.

Fig. 10 shows that the variation in ac conductivity with temperature for PMNZT-CZ10x specimens at a measurement frequency of 1 kHz. It can be broadly into four regions, which are 30–100 °C, 120–280 °C, 280–350 °C and above 350 °C.

In the lower temperature range of 20–100 °C, the p-type and/or n-type hopping charge will be dominant factor in ac conductivity, which gradually increase due to the lower activation energy from 0.07 eV ($x = 0$) to 0.03 eV ($x = 2$) and is insensitive to temperature. As the temperature rises from 120 °C to 280 °C, the polarons from electron and phonon interactions, and oxygen vacancies conduction (cation migration) result in a rapid increase in conductivity with the activation energy is from 0.14 eV ($x = 0$) to 0.10 eV ($x = 2$). Table 3 also lists the activation energy of PMNZT-CZ10x specimens at a frequency of 100 Hz, for the temperature ranges 30–100 °C and 120–280 °C. The variation in E_a with respect to both frequency and temperature shows similar results.

As temperature further increases between 280 °C and 350 °C and approaches to the Curie temperature, there is a phase transition, from ferroelectric structure to paraelectric structure. As would be expected from the conduction models and structural deformations already discussed, this leads to a sharp increase. As the further temperature exceeds 350 °C, the PMNZT-CZ10x specimens are beyond the Curie temperature and the conductivities rapidly enter the paraelectric region, resulting in the negative temperature conductance. These results agree with reported literatures.[20,35,36]

From Table 3 and Fig. 10, the ac conduction activation energy of the ZnO doped PMNZT-C specimens are lower at high frequency than at lower frequency. This is attributable to the fact that at the lower frequency, the conductivity is mainly due to the mobility or transportation over long distance, rather than relaxation or orientation. The energy required for the relaxation or orientation process is lower than that required for transport of a charge carrier over longer distance. The lower activation energy obtained at high temperatures is attributable to the thermal motion of the oxygen vacancies, or the formation of associations between oxygen vacancies and residual cations, at the grain boundary.[37]

From Figs. 9 and 10, it can be concluded that in the lower temperature region, ac conductivity is substantially higher than the dc conductivity due to a lower activation energy. The variation in conductivity shows that the great doping amount of ZnO mainly enters the B-site of the perovskite structure and affects the electrical properties of specimens by inducing the formation of oxygen vacancies for the charge compensation. However, the exact amounts of ZnO entering the A and/or B site of the perovskite structure will be investigated in the future, using the conductivity analysis.

Table 3
dc and ac activation energy versus temperature (30–280 °C) for the PMNZT-CZ10x specimens, using the least square fit by the linear approximation equation $y = mx + b$ (where $y = \ln\sigma$, $x = 1000/T$ and $m = -E_a/(1000\,\mathrm{KT})$ from Arrhenius equation.

Parameters	Temperature range	ZnO (x wt.%) additive				
Ea (eV)		0	0.1	0.5	1	2
dc	30–100 °C	0.14	0.13	0.30	0.34	0.35
dc	120–280 °C	0.67	0.75	0.67	0.65	0.66
ac (100 Hz)	30–100 °C	0.12	0.14	0.06	0.06	0.05
ac (100 Hz)	120–280 °C	0.26	0.35	0.32	0.31	0.30
ac (1 kHz)	30–100 °C	0.08	0.10	0.05	0.04	0.03
ac (1 kHz)	120–280 °C	0.16	0.24	0.20	0.19	0.17

Fig. 11 shows the dc and ac conductivity of PMNZT-CZ10 ($x = 0.1$) at measurement frequencies of 0.1 k, 1 k, 10 k, and 100 kHz. It can be seen that in the higher temperature region above Curie temperature, the ac conductivity shows strong temperature dependence but is almost frequency independence. The dc conductivity gradually approximate to the ac conductivity and then will be merged together. The behavior of dc conductivity in the higher temperature region is explained by the very short relaxation time, which allows the ac conductivity to remain independent of frequency variation.[20] The ac conductivity is almost independent of temperature in the lower region (<200 °C), but it markedly increases in the high temperature due to the phase structure transformation occurred (tetragonal phase to cubic phase).

Fig. 12 shows the frequency dependence of the ac conductivity as a function of ZnO contents, at room temperature. As can be observed, the ac conductivity in a specific temperature and frequency range obeys the Jonscher power law as followed[38]

$$\sigma_{ac}(T,\ \omega) = A(T)\,\omega^{s}$$

where A is a temperature-dependent constant, and s is the exponent within $0 < s \leqq 1$. Funke[39] explained that the value of s might have a physical meaning. As $s \leqq 1$, it means that the hopping motion involved is a translational motion with a sudden hopping. While as $s > 1$, it means that the motion involved is a localized hopping of the species with a small hopping without movement outside the neighborhood.

To validate the above mechanism, the inset of Fig. 12 shows the s values for specimens with various ZnO contents calculated using the Jonscher relation with least square fitting of the data. It can be seen that the s value slightly increases with increasing ZnO contents except specimens for $x = 0$ and 0.01 ($s = 1.52$ and 1.08, respectively). Other specimens comply with the Jonscher power law within the range $0 < s \leqq 1$ for $x = 0.5$, 1.0, and 1.5 at room temperature.

3.4. Piezoelectric properties and electrical conductivity interrelation

The electro-mechanical properties of the PMNZT-CZ10x specimens, taken from previous studies[12], are listed in Table 4. It can be seen that as the suitable amount of ZnO additive yields improved piezoelectric properties in k_p, k_t by the modified mixed-oxide method over the conventional mixed-oxide method. These improved piezoelectric performance is possibly attributable to the deformation in the crystal structure (Table 1), and the chemical homogeneity.[7] The ac conductivity analyses (Figs. 10 and 11) and piezoelectric properties (Table 4) of the

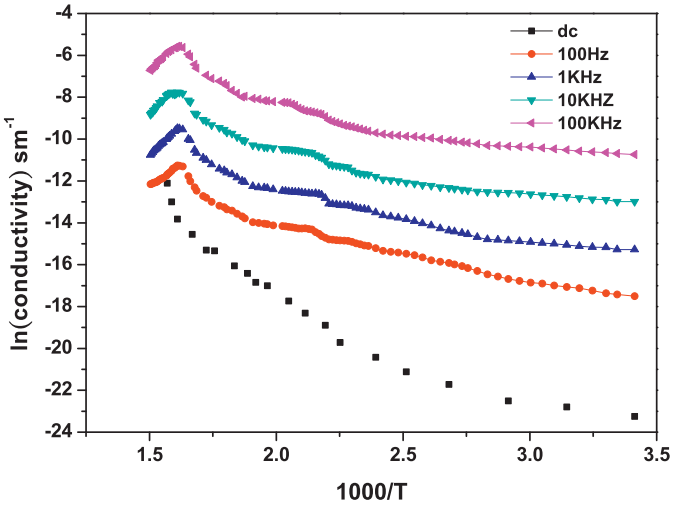

Fig. 11. dc and ac conductivity as a function of 1000/T variation ranging from 300 °K to 600 °K for PMNZT-CZ10x specimens at measured frequency 0.1 k, 1 k, 10 k, 100 kHz.

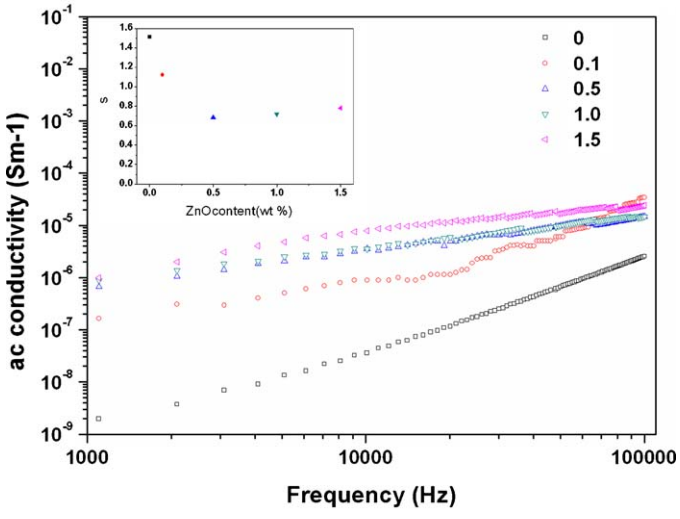

Fig. 12. Frequency dependence of the ac conductivity as a function of ZnO contents at room temperature for $x = 0$, 0.1, 0.5, 1, 1.5 in the measured frequency range of 1 k–100 kHz.

Table 4
Properties of the piezoelectric ceramics for PMNZT-CZ10x composition sintered at 980 °C.

composition	Dielectric constant (ε_r) at 1 kHz	Dielectric loss ($\tan\delta$) at 1 kHz	Sintering temperature (°C)	K_p	K_t	Q_m	ac conductivity $\times 10^{-7}$ (s m^{-1})
PMNZT-C[a]	900	0.6	1020	0.54	0.47	850	3.5
PMNZT-CZ10x[b]							
$x=0$	780	0.45	980	0.48	0.47	1450	2.48
$x=0.1$	960	0.47	980	0.54	0.51	1280	2.45
$x=0.5$	970	0.80	980	0.56	0.55	820	4.72
$x=1$	980	1.85	980	0.53	0.53	680	6.88
$x=2$	940	1.8	980	0.52	0.50	635	11.05

[a] Represents mixed-oxide method.
[b] Represents modified mixed-oxide method (combined mixed-oxide and wolframite method), ac conductivity measured at frequency of 10 kHZ.

specimens show that the ac conductivity of specimens is higher than that of un-doped specimens, the Q_m, is markably degraded, but the k_p and k_t are improved due to the increase in space polarization increasing, when $x<1$. Further increasing x beyond 1 wt.%, the values of k_p and k_t decrease because the ZnO segregation at the grain boundary decreases the piezoelectric activity.

In order to produce high performance in piezoelectric power devices, it is important to give careful consideration to the relationship between the ac conductivity and the piezoelectric activity and mechanical quality factor. As a result, the preferred level of ZnO doping for PMNZT-CZ10x specimens is for the value, $x=0.1$. This concentration suggests that the low ac conductivity is another important factor for use in the high power applications.

4. Conclusion

The low-temperature sintered piezoelectric ceramics with compositions of PMNZT-CZ10x ($0 \leqq x \leqq 2$) were prepared, using the modified mixed-oxide method. As the amount of ZnO increases, the phase transformation in the perovskite structure gradually exhibits more tetragonal phase. The diffusiveness γ (or degree of disorder) of dielectric constant distribution decreases with increasing the amount of ZnO additive from 1.95 ($x=0$) in the DPT to 1.06 ($x=2$) in the normal ferroelectrics. There is not obvious frequency dispersion at the maximum dielectric peak temperatures for the ZnO-doped PMNZT-C specimens.

The variation in conductivity with temperature obeys the Arrhenius law, and the ac conductivity complies with the Jonscher power law for $x=0.5$, 1, and 1.5. As $x<1$, the ac activation energy is decreased with increasing the amount of ZnO for the ZnO-doped PMNZT-C specimens. The corresponding conductivity and electro-mechanical properties are increased, while the mechanical quality factor is reduced. In addition, the correlation between conductivity and piezoelectric properties suggests that the lower ac conductivity of specimens is the critical factor for high power applications.

References

1. Jaffe B, Cook Jr WR, Jaffe H. *Piezoelectric Ceramics*. London, New York: Academic Press Limited; 1971.
2. Tressler J, Alkoy FS, Newnham RE. Piezoelectric sensors and sensor materials. *J Electroceram* 1998;**2**:257–72.
3. Takahashi M, Tsubouchi N, Yonezawa M, Ohno T, Akashi T. Piezoelectric properties of ternary ceramic compounds consisting either of $Pb(Mn_{1/3}Nb_{2/3})O_3$ or $Pb(Mn_{1/2}Nb_{1/2})O_3$ with $PbTiO_3$-$PbZrO_3$. *NEC Res Dev* 1974;**20**:57–60.
4. Park JH, Kim BK, Song KH, Park SJ. Piezoelectric properties of Nb_2O_5 doped and MnO_2-Nb_2O_5 co-doped $Pb(Zr_{0.53}Ti_{0.47})O_3$. *J Mater Sci Mater Electron* 1995;**6**:97–101.
5. Chen H, Guo X, Meng Z. Processing and properties of PMMN-PZT quaternary piezoelectric ceramics for ultrasonic motors. *Mater Chem Phys* 2002;**75**:202–6.
6. Satoh ISEQ, Mamiya KY. High power characteristics of piezoelectric ceramics in $Pb(Mn_{1/3}Nb_{2/3})O_3$-$PbTiO_3$-$PbZrO_3$ system. *Jpn J Appl Phys* 1999;**38**:5531–4.
7. Tsai CC, Chiang TK, Chu SY. The improvement of dynamic characteristics of ultrasonic therapeutic transducer using fine-grain PZT-based piezoceramics. *IEEE Trans Ultrason Ferroelectr Freq Control* 2009;**56**(1):556–66.
8. Priya S, Kim HW, Uchino K. Low temperature coefficient of resonance frequency composition in system Pb(Zr Ti)O_3-$Pb(Mn_{1/3}Nb_{2/3})O_3$. *J Am Ceram Soc* 2004;**87**:1907–11.
9. Yang CF, Wu L, Wu TS. Effect of CuO on the sintering and dielectric characteristics of $(Ba_{1-x}Sr_x)(Ti_{0.9}Zr_{0.1})O_3$ ceramics. *J Mater Sci* 1992;**27**:6573–8.
10. Kim DW, Ko KH, Hong KS. Influence of copper (II) oxide additions to zinc niobate microwave ceramics on sintering temperature and dielectric properties. *J Am Ceram Soc* 2001;**84**:1286–90.
11. Corker DL, Whatmore RW, Ringgaard E, Wolny WW. Liquid-phase sintering of PZT ceramics. *J Eur Ceram Soc* 2000;**20**:2039–45.
12. Tsai C-C, Chu S-Y, Lu C-H. Doping effects of CuO additives on the properties of low-temperature-sintered PMnN-PZT-based piezoelectric ceramics and their applications on surface acoustic wave devices. *IEEE Trans Ultrason Ferroelectr Freq Control* 2009;**56**(3):660–8.
13. Hagha MN, Kerman K, Jadidian B, Safari A. Dielectric and piezoelectric properties of Cu^{2+}-doped alkali niobates. *J Eur Ceram Soc* 2009;**29**:2325–32.
14. Ha J-Y, Choi J-W, Kang C-Y, Choi DJ, Kim H-J, Yoon S-J. Effects of ZnO on the piezoelectric properties of 0.01PMW-0.41PNN-0.35PT-0.23PZ ceramics. *Mater Chem Phys* 2005;**90**:396–400.
15. Ahn C-W, Song C-W, Nahm S, Priya S, Park S-H, Uchino K, Lee H-G, Lee H-J. Effect of ZnO and CuO on the sintering temperature and piezoelectric properties of a hard piezoelectric ceramic. *J Am Ceram Soc* 2006;**89**:921–5.
16. Yoon M-S, Kim Y-M, Kweon S-Y, Hong T-W, Lee Y-G, Ryu S-L, Kim H-J, Ur S-C. Effects of ZnO on the piezoelectric properties of $Pb(Mn_{1/3}Sb_{2/3})O_3$-Pb(Zr Ti)O_3 ceramics. *J Electroceram* 2007;**18**:73–5.
17. Rubio-Marcos F, Romero JJ, Navarro-Rojero MG, Fernandez JF. Effect of ZnO on the structure, microstructure and electrical properties of KNN-modified piezoceramics. *J Eur Ceram Soc* 2009;**29**:3045–52.
18. Nabunmee S, Rujijanagui G, Vittayakom N, Cann DP. Observation of high dielectric constants in $xPb(Zn_{1/3}Nb_{2/3})O_3$-(0.2-x)$Pb(Ni_{1/3}Nb_{2/3})O3$-$0.8Pb(Zr_{1/2}Ti_{1/2})O_3$ ternary solid solutions. *J Appl Phys* 2007;**102**:094108.

19. Vittayakom N, Puchmark C, Rujijanagui G, Tan X, Cann DP. Piezoelectric properties of (1-x)Pb($Zr_{1/2}Ti_{1/2}$)O3-x Pb($Zn_{1/3}Nb_{2/3}$)O_3 ceramics prepared by the columbite-(wolframite) precursor method. *Curr Appl Phys* 2006;**6**:303–6.
20. Portelles J, Almodovar NS, Fuentes J, Raymond O, Heiras J, Siqueiros JM. ac conductivity in Gd doped Pb($Zr_{0.53}Ti_{0.47}$)O3 ceramics. *J Appl Phys* 2008;**104**:073511.
21. IEEE Standard on Piezoelectricity ANSI/IEEE Standard 176-1987. *The Institute of Electrical and Electronics Engineers*. New York; 1987.
22. Valant M, Suvorov D, Pullar RC, Sarma K, Alford NM. A mechanism for low-temperature sintering. *J Eur Ceram Soc* 2006;**26**:2777–83.
23. Boutarfaia A. Investigations of co-existence region in lead zirconate-titanate solid solution: X-ray diffraction studies. *Ceram Inter* 2000;**26**:583–7.
24. Chen YH, Uchino K, Viehland D. Substituent effects in 0.65Pb($Mg_{1/3}Nb_{2/3}$)O_3-0.35$PbTiO_3$ piezoelectric ceramics. *J Electroceram* 2001;**6**:13–9.
25. Vittayakorn N, Rujijanagul G, Tunkasiri, Tan x, Cann DP. Perovskite phase formation and ferroelectric properties of the lead nickel niobate-lead zinc niobate-lead zirconate titanate ternary system. *J Mater Res* 2003;**18**:2882–9.
26. Park SH, Ahn CW, Nahm S, Song JS. Microstructure and piezoelectric properties of ZnO-added ($Na_{0.5}K_{0.5}$)NbO3 ceramics. *Jpn J Appl Phys* 2004;**43**(8B):L1072–4.
27. Li H, Yang Z, Wei L, Chang Y. Effect of ZnO addition on the sintering and electrical properties of (Mn W)-doped PZT-PMS-PZN ceramics. *Mater Res Bull* 2009;**44**:638–43.
28. Okazaki K, Nagata K. Effects of grain size and porosity on electrical and optical properties of PLZT ceramics. *J Am Ceram Soc* 1973;**56**:82–6.
29. Martirena HT, Burfoot JC. Grain-size effects on properties of some ferroelectric ceramics. *J Phys C Solid State Phys* 1974;**7**:3182–92.
30. Randall GA, Kim N, Kucera JP, Gao W, Shrout TR. Instrinsic and extrinsic size in fine-grained morphotropic-phase-boundary lead zirconate titanate ceramics. *J Am Ceram Soc* 1998;**81**:677–88.
31. Uchino K, Nomura S. Critical exponents of the dielectric constants in diffused-phase-transition crystals. *Ferroelectrics* 1982;**44**:53–61.
32. Zhang H, Jiang S, Zeng Y. B site doping effect on depinning in Pb($Mn_{1/3}Nb_{1/3}Sb_{1/3}$)$_x$($Zr_{0.825}Ti_{0.175}$)$_{1-x}$O3 ferroelectric ceramics. *Appl Phys Lett* 2008;**93**:192901.
33. Chao X, Ma D, Gu R, Yang Z. Effects of CuO addition on the electrical responses of the low-temperature sintered Pb(Zr0.52Ti0.48)O3–Pb(Mg1/3Nb2/3)O3–Pb(Zn1/3Nb2/3)O3 ceramics. *J Alloys Compd* 2010;**491**:698–702.
34. Moulson J, Herbert JM. *Electroceramics*. 2nd ed. New York: John Wiley & Sons, Inc.; 2003.
35. Lee JS, Park EC, Lee SH, Lee DS, Lee YJ, Kim JS, Kim IWJBM. Conduction analysis of Li_2O doped 0.2[Pb(Mg1/3Nb2/3)]-0.8[PbTiO3-PbZrO3] ceramics fabricated by columbite precursor method. *Mater Chem Phys* 2005;**90**:381–5.
36. Zhu Z, Jiang K, Davies GJ, Li G, Yin Q, Sheng S. Dielectric relaxation behavior in Pb($Mn_{1/3}Sb_{2/3}$)O3-Pb(Zr Ti)O3 systems. *Smart Mater Struct* 2008;**15**:1249–54.
37. Rao KS, Krishna PM, Prasad DM, Lee JH, Kim JS. Electrical, electromechanical and structural studies of lead potassium samarium niobate ceramics. *J Alloys Compd* 2008;**464**:497–507.
38. Jonscher AK. Dielectric relaxation in solids. *J Phys D* 1999;**32**:R57–70.
39. Funke K. Jump relaxation in solid electrolytes. *Prog Solid State* 1993;**22**:111–5.